Journal of Science: Advanced Materials and Devices xxx (xxxx) xxx

Contents lists available at ScienceDirect

Journal of Science: Advanced Materials and Devices

journal homepage: www.elsevier.com/locate/jsamd

Original Article

Calcium phosphate stability on melt electrowritten PCL scaffolds

Naghmeh Abbasi [a, b], Stephen Hamlet [a, b, **], Van Thanh Dau [c], Nam-Trung Nguyen [d, *]

[a] School of Dentistry and Oral Health, Griffith University, Gold Coast Campus, Southport, QLD 4215, Australia
[b] Menzies Health Institute Queensland, Griffith University, Gold Coast Campus, Southport, QLD 4215, Australia
[c] School of Engineering and Built Environment, Griffith University, Gold Coast Campus, Southport, QLD 4215, Australia
[d] Queensland Micro- and Nanotechnology Centre, Griffith University, Nathan Campus, 170 Kessels Road, 4111, Brisbane, QLD Australia

ARTICLE INFO

Article history:
Received 25 October 2019
Received in revised form
31 December 2019
Accepted 10 January 2020
Available online xxx

Keywords:
Calcium phosphate coating
Polycaprolactone
Melt electrowriting
Apatite mineralization
Plasma treatment
Bone regeneration

ABSTRACT

Calcium phosphate (CaP) coating on melt electrowritten (MEW) substrates is a potential candidate for bone regeneration influencing the interaction of osteoblasts with implanted scaffolds. Pretreatment to improve hydrophilicity of the hydrophobic polymer fibres affects subsequent coating with bioactive compounds like CaP. Therefore, this study evaluated the subsequent stability and structural properties of CaP coated MEW Poly-ε-caprolactone (PCL) scaffolds following pre-treatment with either argon-oxygen plasma or sodium hydroxide (NaOH). Scanning electron microscopy and μ-CT showed uniform CaP coating after one hour immersion in simulated body fluid following plasma pretreatment. Moreover, fourier transform infrared spectroscopy, energy dispersive spectrometry and X-ray diffraction analysis confirmed the presence of hydroxyapatite, tetracalcium phosphate and halite structures on the coated scaffolds. Contact angle measurement showed that the plasma pretreatment and CaP coating improved the hydrophilicity of the scaffold. However, the mechanical properties of the scaffolds were degraded after both plasma and NaOH treatments. The tensile stability was significantly improved following mineralization in plasma-treated scaffolds due to the smaller crystal size formed on the surface resulting in a dense CaP layer. The results obtained by thermogravimetric analysis also confirmed higher deposition of CaP particles on coated scaffolds following plasma modification. The results of this study show that plasma pre-treated mineralized MEW PCL scaffolds are sufficiently stable to be useful for further development in bone regeneration applications.

1. Introduction

The remodeling of the bone tissue around implanted materials is influenced by the surface charge and chemistry of the implanted materials [1]. PCL is a biodegradable polyester widely used as an implantable biomaterial [2]. However for tissue engineering purposes, PCL has some significant shortcomings such as slow degradation rate, hydrophobic properties and low cell adhesion [3]. The incorporation of CaP into PCL has yielded a class of hybrid biomaterials with remarkably improved mechanical properties, controllable degradation rates, and enhanced bioactivity as calcium and phosphate ions are essential for skeletal mineralization where mineral crystals are deposited in an organized fashion onto the organic ECM [4]. Moreover CaP coating imparts an increased surface roughness to coated scaffolds. Rough implant surfaces enhance the contact between the implant and the bone tissue improving subsequent integration [5]. Coating biocompatible substrates with these inorganic crystals has subsequently shown the significant bone growth and vascularization [6] including CaP coated electrospun poly (ethylene oxide terephthalate)–poly(buthylene terephthalate) scaffolds in vivo [7].

Bone calcification and maturation can be stimulated by releasing calcium ions [8]. Calcium and phosphorus ions released from coated scaffolds can adjust the ion concentration and local pH of the environment, affecting protein adhesion, attachment of the osteoblasts and their activation which has an impact on bone regeneration [9]. Following coating, CaP crystal structure, surface area and particle size as well as the temperature, acidity and fluid movement within a coated scaffold can all affect the dissolution process [10,11]. Furthermore, changes to the pore size and pore number in CaP particles will enhance body fluid convection due to better contact between the CaP

* Corresponding author. QLD Micro- and Nanotechnology Centre, Nathan campus, Griffith University, 170 Kessels Road QLD 4111, Australia.
** Corresponding author. School of Dentistry and Oral Health, Griffith University, Gold Coast Campus, QLD 4222, Australia.
E-mail addresses: naghme.k@gmail.com (N. Abbasi), s.hamlet@griffith.edu.au (S. Hamlet), v.dau@griffith.edu.au (V.T. Dau), nam-trung.nguyen@griffith.edu.au (N.-T. Nguyen).
Peer review under responsibility of Vietnam National University, Hanoi.

https://doi.org/10.1016/j.jsamd.2020.01.001

Please cite this article as: N. Abbasi et al., Calcium phosphate stability on melt electrowritten PCL scaffolds, Journal of Science: Advanced Materials and Devices, https://doi.org/10.1016/j.jsamd.2020.01.001

crystal surface area and body fluids [12]. On the other hand, greater porosity also results in poor mechanical properties and CaP coated layers displayed a weak load-bearing capacity [13].

Surface activation by pretreating the substrate material has been reported to affect the rate of coating formation [14]. Various approaches have been tried to improve subsequent CaP deposition onto PCL scaffolds [15] including O_2 plasma treatment [16], chemical modification [17], film deposition [18], thermal and lipase dependent surface modification [19] and etching in alkaline and acidic solutions [20]. Similar methods of activation have been used with electrospun fibrous scaffolds pior to CaP coating e.g. gelatin treated poly lactic-glycolic acid (PLGA) scaffolds to produce positively charged groups [21] and ethanol treatment on electrospun PCL, poly(3-hydroxybutyrate) (PHB) and polyaniline (PANi) polymers [22].

Although other studies demonstrated the production of CaP on solution electrospun scaffolds with nanometer scale fibres (300 nm−1 μm) [7,23,24], no quantitative studies are available comparing the stability characteristics of CaP coated MEW scaffolds with micrometer scale fibres (2−50 μm) following plasma and NaOH pre-treatment. This study shows the great potential of evaluating the CaP stability on the scaffold constructs with larger-sized fibre dimension. Accordingly, our study characterized the effects of NaOH and argon-oxygen (Ar−O_2) plasma pre-treatment on the CaP coated MEW PCL scaffolds using scanning electron microscopy (SEM), fourier transform infrared spectroscopy (FTIR), energy dispersive spectrometry (EDS), micro-CT (μ-CT), thermogravimetric analysis (TGA), X-ray diffraction (XRD), mechanical tests and contact angle as the CaP stability is critically important for later potential bone engineering applications.

2. Materials and methods

The MEW printer used in this study contained a high voltage source (DX250R, EMCO, Hallein, Austria) controlled by a voltage divider (Digit Multimeter 2100, Keithley, Cleveland, USA), a pneumatically regulated melt feeding system (FESTO, Berkheim, Germany) and a planar movable aluminium collector plate (XSlide, Velmex, New York, USA) controlled by G-code (MACH 3 Computerized Numerical Control (CNC) software, ARTSOFT, Livermore Falls, USA). A proportional-integral-derivative controller was used to regulate the electrical heating system (TR400, Delta-t, Bielefeld, Germany) to assure a stable melt temperature profile.

Two grams of medical-grade 80 kDa PCL pellets (Corbion, Australia) was placed in a 2 mL syringe with a 21G nozzle, and heated to 80 °C for 30 min to melt before insertion into the MEW heated head. The feed rate was 20 mL/h, which was controlled via compressed air. A threshold voltage between 5 and 7 kV was applied to create the charged polymer and to form a Taylor cone. The X−Y movement of the collector platform was controlled using programmable software (G-code) that places the deposited polymer fibres in the desired pattern. From our previous studies and other reports [25,26], an optimal scaffold pore size for bone regeneration is in the range of 100−400 μm. In this study, the averagepore size of 250 μm was designed and printed.

MEW PCL scaffolds (2 × 2 cm) were placed in 100% ethanol for 15 min under a vacuum to remove any residual contamination before allocation into one of five treatment groups:

(1) Control group (nC) − non coated; (2) NaOH treatment (Na-nC) − scaffolds immersed in pre-warmed 1 M NaOH at 37 °C for 30 min then washed with Milli Q water until the pH was neutralized; (3) Plasma treatment (Plas-nC) − Ar and O_2 plasma cleaned at 10.15 W for 7 min each side under vacuum (PDC-002-HP, Harrick Plasma, USA); (4) NaOH treatment + CaP coating (Na−C) − NaOH treatment of scaffold as (2) above followed by immersion in highly saturated SBF (10x) solution [27] at 37 °C for 0.5, 1, 3 and 6 h. The SBF was replaced every 30 min. After washing the scaffolds in Milli Q water, they were immersed in 0.5 M NaOH at 37 °C for 30 min. Finally, the scaffolds were rinsed with distilled water then collected for freeze drying overnight; (5) Plasma treatment + CaP coating (Plas-C) − Plasma treatment of scaffold as (3) above followed by SBF as (4) above.

To characterize the surface morphology of the MEW scaffolds, the samples were coated with gold and examined with a scanning electron microscope (Jeol JCM-5000) operating at 15 kV accelerating voltage.

Scaffolds were cut into 6 mm discs using a tissue biopsy punch (kai Europe GmbH, Solingen, Germany) and coated with gold. The elemental analysis was performed by JSM-7800 scanning electron microscope (Japan), equipped with energy dispersive X-ray spectroscopy (INCA, Oxford Instruments, UK).

The scaffold hydrophilicity was assessed by measuring the water contact angle using a Contact Angle and Surface Tension instrument (FTA200, Poly-Instruments Pty. Ltd., Australia) running with the following parameters; pump speed 2 μl/s, needle diameter 0.279 mm, water droplet diameter 1.0 mm. Three different locations on the sample were selected to measure the angle between the surface and a liquid droplet. Images were captured via a CCD video camera running in real time and saved for further analysis.

Tensile strength tests were performed on all five groups of coated and non-coated PCL scaffolds using an electromechanical Micro-Tester (Instron 5848, Norwood, Ma) with a 500 N load cell and a gauge length of 15 mm (5 samples/group). Samples 45 × 10 mm and 1 mm thick were prepared and stretched at a speed of 15 mm/min until breakage. The subsequent slope of each stress−strain curve was analysed.

X-ray diffraction of the scaffolds was recorded using a Cu-$K_{\alpha 1}$ source, λ = 1.5406 Å diffractometer (RigaraSmartLab, Germany) operating at 40 kV, 40 mA. The scanswere performed on powder from 10° to 40° scanning range, a step size of 0.04° and irradiation time of 0.96 s per step. The mean crystallite size was determined using the system software (DIFFRAC SUITE EVA).

FTIR spectroscopy (Bruker Vertex 70 spectrometer) was used to characterize the functional groups on the scaffolds. Four different points on each sample were analysed. The diamond anvil cell (DAC) was placed on the aligned orientation of the sample and screwed until touch the sample. The scan test samples was analysed for chemical properties.

Thermal behaviour of 20 mg of each of the CaP coated PCL scaffolds were examined at a temperature range of 25−600 °C with a heating rate 10 K min^{-1} (Netzsch Jupiter Simultaneous Thermal Analyser, Germany).

The distribution of CaP in the scaffolds was examined by μ-CT. A 6-mm disc of each scaffold was placed inside the X-ray tube of a micro-CT scanner (μCT40, SCANCO Medical AG, Brüttisellen, Switzerland) and exposed to 55 kV of X-rays with a current of 120 μA. Analysis was performed using a greyscale threshold of 10 and resolution of 6 μm. The μ-CT software package was used for 3D visualization of the scaffolds reconstructed from the 2D scanned slices. The fibres showing in grayscale images were eliminated by selecting a suitable threshold corresponding to the CaP particle distribution. The volume of mineralisation in the test constructs (Na−C and Plas-C) was approximated by subtracting the mean volume of the control (nC) scaffold using CTAn program.

All data were expressed as mean ± standard deviation. Comparisons between groups were analysed by analysis of variance (ANOVA, post hoc test: Tukey). The statistical software SPSS 17.0 for windows was used for calculations and $p < 0.05$ was considered to be statistically significant.

Please cite this article as: N. Abbasi et al., Calcium phosphate stability on melt electrowritten PCL scaffolds, Journal of Science: Advanced Materials and Devices, https://doi.org/10.1016/j.jsamd.2020.01.001

3. Results

3.1. Morphological characterization of scaffolds (SEM)

SEM images of the scaffold structures showed that the scaffolds retained their porous nature after CaP coating (Figure S1). 0.5 h SBF treatment did not fully cover the whole fibre surface (Figure S1-a), while immersion for 1 h provided uniform coating of the structures in both Na–C and Plas-C groups (Figure S1-b). Morphologically, the CaP clusters formed were more spherical in arrangement on the Na–C scaffold (Figure S1-b2) in comparison with Plas-C scaffold, where they were distributed smoothly (Figure S1-b4). After 3 and 6 h immersion in SBF, there was an increase in crystalline deposition and a thick layer of CaP

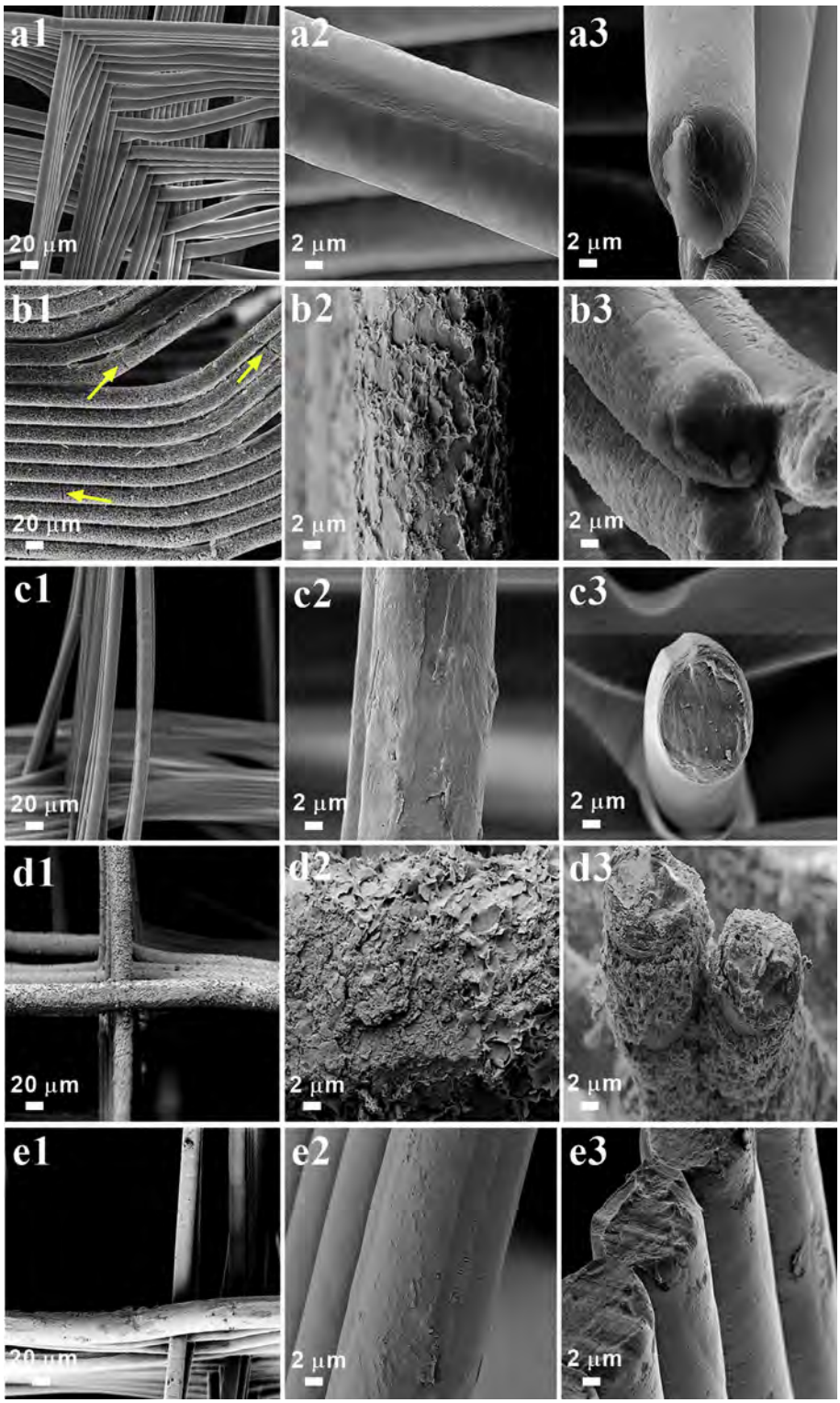

Fig. 1. SEM images of CaP coated scaffolds following immersion in SBF for 1 h at low (1) and high magnification (2,3) showing the morphology of scaffold samples: (a) nC, (b) Na–C, (c) Na-nC, (d) Plas-C, (e) Plas-nC.

Please cite this article as: N. Abbasi et al., Calcium phosphate stability on melt electrowritten PCL scaffolds, Journal of Science: Advanced Materials and Devices, https://doi.org/10.1016/j.jsamd.2020.01.001

Table 1
Elemental analysis (% weight) of coated and non-coated MEW PCL scaffolds: nC; Na–C; Na-nC; Plas-C; Plas-nC.

Element	nC (% weight)	NaOH–C (% weight)	NaOH-nC (% weight)	Plasma-C (% weight)	Plasma-nC (% weight)
Ca	–	2.7	–	6.7	–
P	–	–	–	1.7	–
Na	–	7.0	–	2.2	–
K	–	–	–	1.5	–
Mg	–	–	–	0.4	–
Cu	–	–	–	1.3	0.4
Al	8.0	1.8	100	2.1	6.9
O	92.0	74.6	–	71.7	92.6
Cl	–	13.9	–	12.4	–

particles encased the fibres which reduced the scaffold pore size (Figure S1-c, d).

Fig. 1-a showed the morphology of PCL surface scaffold before CaP coating (nC). The coating structure in Na–C scaffolds showed some cracks and separation of the coated layer from the fibres after immersion for 1 h (Fig. 1-b1, yellow arrows) whereas a dense evenly coated layer appeared on the Plas-C scaffolds (Fig. 1-d1). NaOH or $Ar–O_2$ plasma treatment alone did not appear to have any significant impact on the fibre diameter (Fig. 1-c, e) although some degradation and peeling of the outer layer of the Na-nC scaffold was apparent (Fig. 1-c2). Also, the surface of Plas-nC scaffold displayed a relatively rough morphology with nanometre features on the surface of the fibres (Fig. 1-e2).

3.2. Elemental characterization (EDS)

EDS analysis identified the proportion of elements found on the scaffold areas through percentage in weight. As expected EDS analysis showed the presence of calcium on the surface of both Na–C and Plas-C scaffolds (Figure S2, Table 1). Pre-treatment with $Ar–O_2$ plasma however increased the level of Ca to 6.7% in Plas-C compared to 2.7% in the Na–C group (was treated with NaOH). Phosphorous however was not detected in Na–C scaffold while it was 1.7% in the Plas-C scaffolds suggesting pre-treatment with $Ar–O_2$ plasma may influence the Ca/P ratio. Sodium as expected was higher in Na–C (7.0%) than Plas-C scaffolds (2.2%). Also, the Plas-C scaffold showed the presence of K and Mg ions which were not found on the other scaffolds. The presence of Copper was observed in both Plas-nC and Plas-C scaffolds.

3.3. Surface evaluation by contact angle (CA)

The hydrophilicity of the treated and untreated scaffolds was assessed by contact angle measurement (Fig. 2). We observed that nC scaffolds showed the hydrophobic nature of PCL with an average contact angle of 135° ± 4.9° (Fig. 2-a). CaP coating significantly increased hydrophilicity of the scaffold surface (CA = 0°) in both Na–C and Plas-C groups (Fig. 2-b, d). Treatment with 1M NaOH only slightly decreased the contact angle (91° ± 12.4°) in Na-nC scaffolds (Fig. 2-c) wheras Plasma treatment alone also significantly increased hydrophilicity of the Plas-nC scaffolds surface (CA = 0°) (Fig. 2-e).

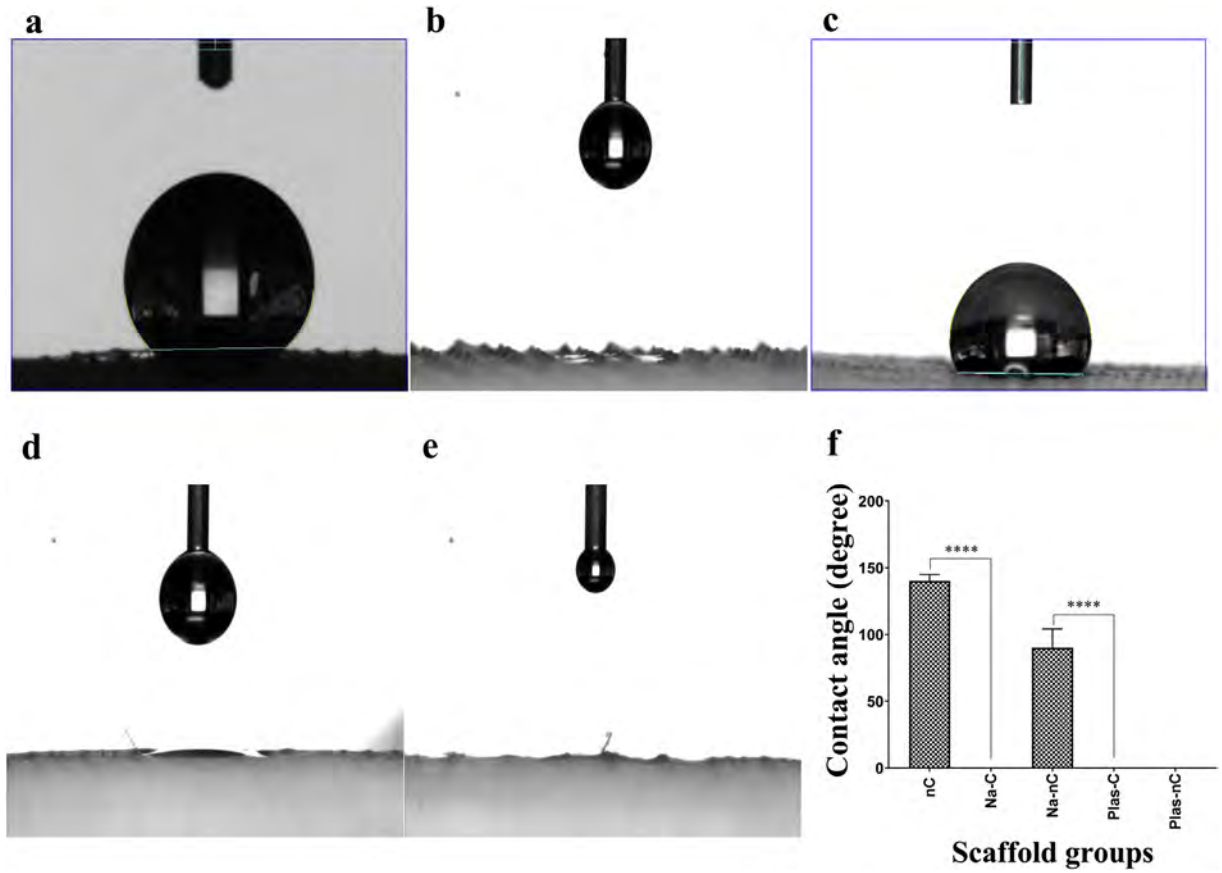

Fig. 2. Water contact angle of PCL scaffolds: (a) nC; (b) Na–C; (c) Na-nC; (d) Plas-C; (e) Plas-nC; (f) Quantitative analysis of hydrophilicity of coated and non-coated scaffolds.

Please cite this article as: N. Abbasi et al., Calcium phosphate stability on melt electrowritten PCL scaffolds, Journal of Science: Advanced Materials and Devices, https://doi.org/10.1016/j.jsamd.2020.01.001

3.4. Mechanical properties

Assessment of the mechanical performance of the PCL scaffolds was carried out and the mechanical properties were calculated from the curve (Fig. 3, Table S1). Apparent stress-strain relationships were recorded (Fig. 3-a) and the Young's modulus of nC scaffold (1.93 ± 0.23 kPa) was shown to be the highest of the scaffold groups. Plas-nC and Na-nC scaffolds both markedly reduced Young's modulus (0.57 ± 0.27 and 0.85 ± 0.47 kPa respectively). Subsequent CaP coating of the plasma treated samples however almost restored the Young's modulus to pretreatment levels (Plas-C 1.67 ± 0.76 kPa) in contrast to Na–C samples where the Youngs modulus was only increased minimally after coating (Fig. 3-b).

The nC scaffold also showed the highest elongation failure value (1088.2 ± 121.4%) and ultimate tensile strength (29.66 ± 1.37 kPa) compared to the other scaffolds (Fig. 3-c, d, Table S1). Similar to the Youngs modulus results, plasma and NaOH treatments again decreased elongation failure values and ultimate tensile strength, but these indicators of tensile strength were able to be partially restored by coating with CaP. Overall, the nC and Plas-nC scaffolds showed the highest and the lowest potential to tolerate tensile loading ($p \leq 0.002$), respectively.

3.5. X-ray diffraction (XRD) analysis

XRD spectra of the scaffolds are shown in Fig. 4. The diffraction peaks at $2\theta = 21.60°$ and 23.95° (asterisks) attributed to PCL were seen in all groups. The absence of crystalline CaP revealed that no coating materials were found in nC specimens. Major pattern peaks at $2\theta = 31.73°$, 66.34° and 75.12° (triangle) could be assigned to the halite structure of NaCl while diffraction peaks at $2\theta = 11.92°$, 29.74° and 34.01° (dot) corresponded to the formation of the

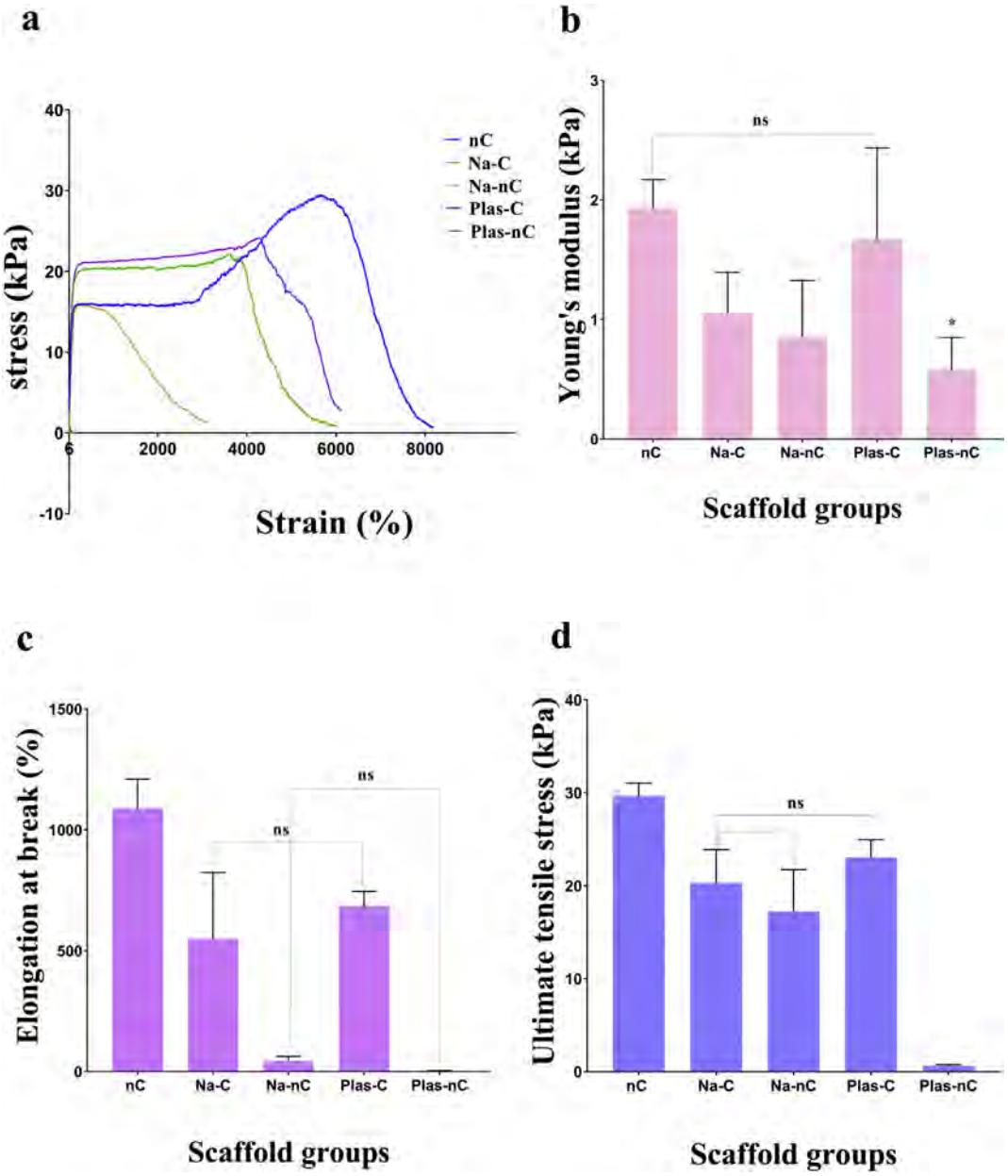

Fig. 3. Mechanical properties of MEW PCL scaffold groups nC; Na–C; Na-nC; Plas-C; Plas-nC. (a) Tensile stress–strain curves; (b) Young's modulus; (c) Elongation at break; (d) Ultimate tensile strength. ns: nonsignificant; *$p \leq 0.002$.

Please cite this article as: N. Abbasi et al., Calcium phosphate stability on melt electrowritten PCL scaffolds, Journal of Science: Advanced Materials and Devices, https://doi.org/10.1016/j.jsamd.2020.01.001

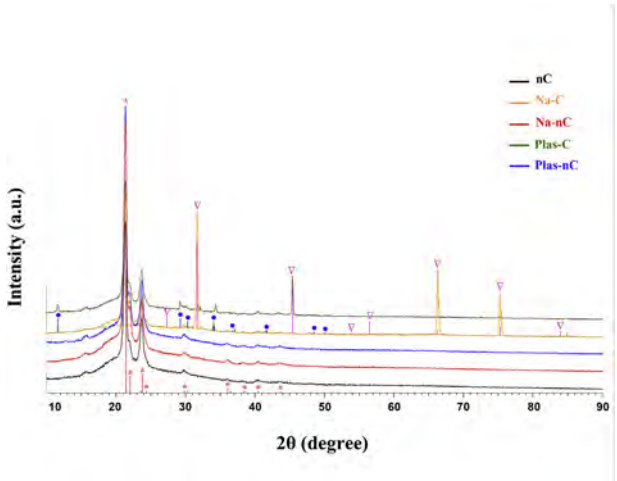

Fig. 4. X-ray diffraction spectra of the MEW PCL scaffolds: nC; Na–C; Na-nC; Plas-C; Plas-nC. *: (C6H10O2)n PCL | Poly-ε-caprolactone, Δ: NaCl halite, ●: HCa(PO4)2(H2O)2 brushite.

phosphate mineral 'brushite' ($HCa(PO_4)_2(H_2O)_2$) seen in the coated scaffolds (Na–C and Plas-C).

Halite and brushite crystalline forms were distinguished in Plas-C and Na–C scaffolds by their difference in crystal orientation (200 for Na–C and 220 for Plas-C scaffolds). In addition, the crystals looked sharp in shape and larger in size for the Na–C scaffolds. Approximately 36.77% halite and 63.23% brushite structures were found in Plas-C scaffolds. The crystal sizes of both coated scaffolds (Na–C and Plas-C) were determined by Scherrer's equation and the average crystal sizes were; PCL (11.72 ± 0.23 nm), halite (44.53 ± 2.76 nm), brushite (50.93 ± 14.44 nm for Plas-C scaffolds and PCL (11.60 ± 0.12 nm), halite (237.27 ± 121.67 nm), brushite (41.63 ± 6.14 nm) for Na–C scaffolds.

Although some small crystalline structures were observed in Na-nC and Plas-nC scaffolds, the absence of crystalline CaP in Na-nC and Plas-nC scaffolds demonstrated this was not due to the coating materials.

3.6. FTIR analysis

Fig. 5 presents the FTIR spectra of the PCL scaffold groups. In nC scaffold, peaks associated with C–O–C at 1161 cm^{-1},C–O–C at 1239 cm^{-1},C–O and C–C at 1293 cm^{-1}, carbonyle stretching at 1721 cm^{-1}, CH_2 stretching at 2946 cm^{-1} and CH_2 stretching at 2866 cm^{-1} were identified.

The FTIR spectra of CaP on the surface of Na–C scaffold group, showed bands corresponding to OH^- stretching at 3341 cm^{-1}, asymmetric PO_4^{3-} bending at 558 and 603 cm^{-1}, asymmetric PO_4^{3-} stretching at 1026 cm^{-1} and symmetric PO_4^{3-} stretching at 959 cm^{-1}.

Hydrophilic groups at 2942 cm^{-1} were identified on the surface of the Na-nC scaffold while for the Plas-C scaffolds, the following absorption bands were identified; OH^- stretch at 3366 cm^{-1}, asymmetric PO_4^{3-} bend at 564 cm^{-1}, symmetric P–O stretch at 960 cm^{-1} and asymmetric PO_4^{3-} stretch at 1045 cm^{-1}. The hydrophilic OH bands at 2943 cm^{-1} corresponded to the surface of the Plas-nC scaffold.

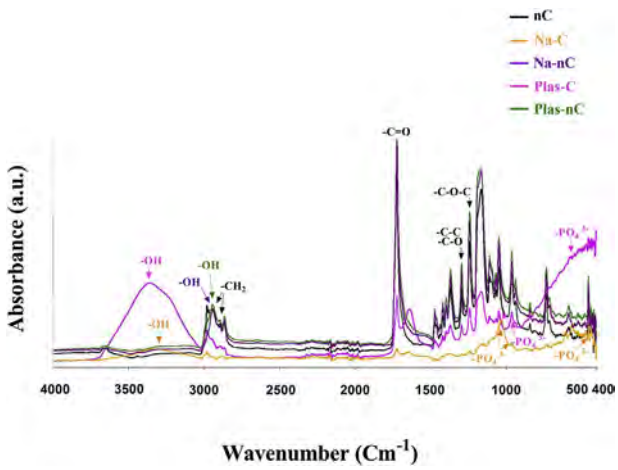

Fig. 5. Fourier-transform infrared spectrum of MEW PCL scaffolds; nC; Na–C; Na-nC; Plas-C; Plas-nC.

3.7. Thermal analysis (TGA)

The TGA-DSC curves of the CaP coated scaffolds (na-C and Plas-C) were obtained under N_2 atmosphere (Fig. 6). Weight loss occured over three temperature ranges as detailed in Table 2 and Figure S3. The first temperature range (25–193.4 °C) was associated with a mass loss of 0.45% for the Na–C scaffold and 0.86% for the Plas-C scaffold at the endothermic peak of 64.9 °C. The preliminary decomposition occurred in the range 193.4–431 °C with a weight loss of 41.66% and 39.15% for the Na–C and Plas-C scaffolds respectively at the maximum peak temperature of 390.3 °C and 393.3 °C respectively. Further decomposition occurred between 431.5 and 600 °C with the highest exothermic peak of 517.9 and 514 °C for Na–C and Plas-C scaffolds respectively. Following the complete degradation of the material, the residual CaP particles was 58.23% and 56.38% for Plas-C and Na–C scaffolds respectively at 600 °C.

3.8. Characterization of PCL scaffolds coated with CaP (μ-CT)

The effect of the different coating treatments was evaluated using μ-CT to determine the distribution of CaP particles within the scaffolds (Fig. 7). No CaP coating was identified in the control (nC), Na-nC and Plas-nC scaffolds (Fig. 7-a, c & e respectively).

The Na–C scaffold showed a heterogeneous distribution of CaP where some areas contained more concentrated CaP, which was aggregated creating some large CaP clusters, whilst other regions were empty of CaP particles (Fig. 7-b). In contrast, the Plas-C scaffolds indicated an even distribution of CaP coating on the surface of the PCL scaffold struts that were spread throughout the inner and outer of scaffold structure (Fig. 7-d).

The total coated mineral volume was significantly increased in Plas-C scaffolds compared to the Na–C scaffolds (40.21 mm^3 in comparison with 31.54 mm^3) (Fig. 7-f).

4. Discussion

CaP is a biomimetic compound widely used in bone tissue engineered applications [19]. Because of the nucleation potential of phosphate and calcium ions, there is a demand for a firm and uniform coating of them onto the scaffold surface. To achieve this, polycaprolactone, a widely used scaffold material, can be surface activated by alkali, acid or plasma pre-treatment [28,29].

This study examined both NaOH and Ar–O_2 plasma treatment of PCL which have been shown to markedly improve the hydrophilicity of PCL. While Ar plasma alone may be preferable for surface cleaning compared to O_2 plasma, as it has less impact on the substrate's material properties [30], an Ar–O_2 plasma mixture has been shown to be more efficient at increasing sample roughness than Ar exclusively [31], which also enhances the adsorption of CaP [32].

Please cite this article as: N. Abbasi et al., Calcium phosphate stability on melt electrowritten PCL scaffolds, Journal of Science: Advanced Materials and Devices, https://doi.org/10.1016/j.jsamd.2020.01.001

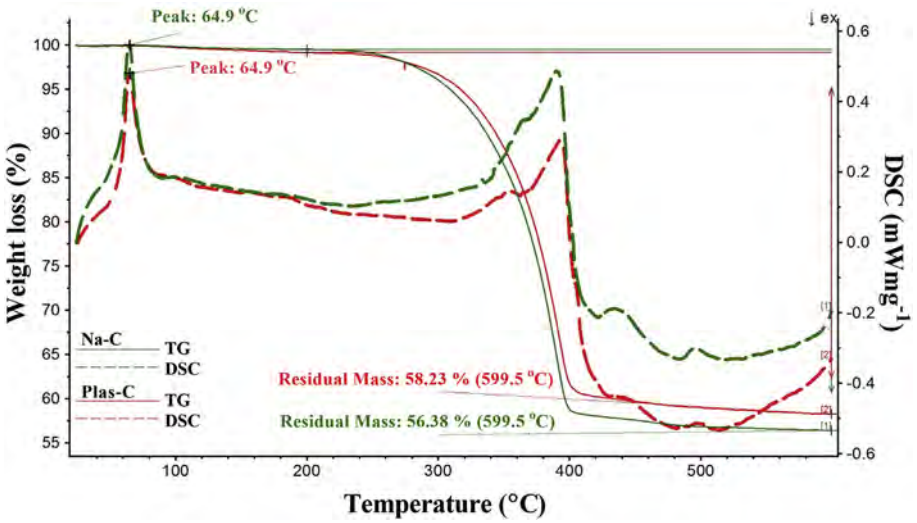

Fig. 6. The TGA-DSC curves of CaP coated MEW PCL scaffolds: Na−C; Plas-C.

However the processes of plasma spraying and etching by NaOH, may significantly alter the material properties of PCL before the coating with CaP. Our SEM data showed that Ar−O_2 plasma treatment significantly increases the surface roughness of the PCL fibres. This is in agreement with previously reported similar studies which showed the surface roughness of a graphite/polymer composite and a porous PCL scaffold also increased with O_2 plasma modification [33]. Also, the study of Lin et al. showed the rough surface of porous PCL scaffolds due to plasma treatment [17].

Mild alkaline conditions in contrast to acidic treatment has been shown to be more beneficial as a substrate pretreatment process, generating less undesirable by-products [34]. While, a dilute NaOH solution was used in this study, its corrosive nature still resulted in the surface layer of the PCL fibres peeling off to create a rough surface, similar to Luickx et al. who also used 1M NaOH on electrospun PCL scaffolds [35]. However, FDM PCL/graphene 3D printed scaffolds were shown to be resistant to 3 h exposure to 5M NaOH [36]. This suggests that NaOH treatment of electrospun mesh-like structures are more vulnerable to cleavage of carboxyl and hydroxyl chains in PCL polymers compared with the fibres of FDM scaffolds.

Following CaP coating, the SEM data showed the Plas-C scaffolds had a uniform coating density without any cracks or fractures compared to the brittle coated layers seen in the Na−C scaffolds and other reported studies where non-uniform surface activation with NaOH treatment resulted in subsequent uneven CaP deposition [17,33]. This was also confirmed by the μ-CT evaluation where large aggregated non-uniform CaP crystals were detected on the surface of Na−C scaffolds compared to the smooth coated Plas-C scaffold.

It is not fully understood what are the main factors i.e. physical (Van der Waals), chemical or mechanical interaction which influences coating adhesion to its substrate [37]. The surface of PCL polymers become super-active by the action of carbonyl (−CO−), carboxyl (−COO−) and hydroxyl (−OH) anions and these negatively charged groups are then ready to attract the soluble positive calcium ions of the SBF solution [38]. The uneven CaP coated layer achieved from Na−C may be due to scaffold pores which were already filled with air and thus not able to take up the aqueous NaOH solution. In contrast, plasma pre-treatment could overcome this limitation by stimulating a homogeneous activation on MEW PCL scaffolds prior to immersion in SBF solution.

Following NaOH and Ar−O_2 plasma treatment, the samples had a negatively charged surface potential able to interact with the positively charged Ca^{2+} ions in the SBF solution. EDS analysis clearly showed the Ca^{2+} content was enhanced in both Na−C and Plas-C scaffolds. However, the percentage of Ca^{2+} ions was higher in Plas-C scaffolds compared to Na−C scaffolds. The positive charge as a result of accumulation of Ca^{2+} ions is then ready to interact to the oppositely charged PO_4^{3-} ions which was observed in Plas-C group. Poorly crystallized CaP and no phosphorus element however was detected by EDS analyses of Na−C scaffolds.

Furthermore, EDS results demonstrated higher concentrations of Na^+ (7.0%) in Na−C scaffolds in contrast to Plas-C scaffolds (2.2%).

Rather the most intense peaks of the XRD analysis identified large deposits of halite structures. Our results showed the molar ratio of Na/Cl was 0.50 for Na−C scaffolds and 0.17 for Plas-C groups. The molar ratio of Na/Cl of less than 1 indicated the removal of Na^+ ions in both scaffold groups. According to the XRD graphs, the main crystal structures of the Plas-C samples were brushite ($CaHPO_4$, $2H_20$), and hydroxyapatite (HAP). While an equal ratio of calcium and phosphate ions represents the brushite structure, the Ca/P ratio in this study was 3.94 for Plas-C scaffolds, which was close to biphasic combinations of HAP (Ca/P: 1.67) and tetracalcium phosphate (TTCP) (Ca/P: 2.00). The mixture of phases of particles resulted in different morphologies of coated pieces that

Table 2
TGA-DSC analysis of CaP coated MEW PCL scaffolds.

Sample	Temperature range (°C)	Mass loss (wt %)	Total mass loss (mg)	DSC peak (°C)
Na−C	25−193.4	0.45	6.46	64.9
	193.4−431.5	41.66		390.3
	431.5−600	1.46		517.9
Plas-C	25−193.4	0.86	5.87	64.9
	193.4−431.5	39.15		393.3
	431.5−600	1.76		514

Please cite this article as: N. Abbasi et al., Calcium phosphate stability on melt electrowritten PCL scaffolds, Journal of Science: Advanced Materials and Devices, https://doi.org/10.1016/j.jsamd.2020.01.001

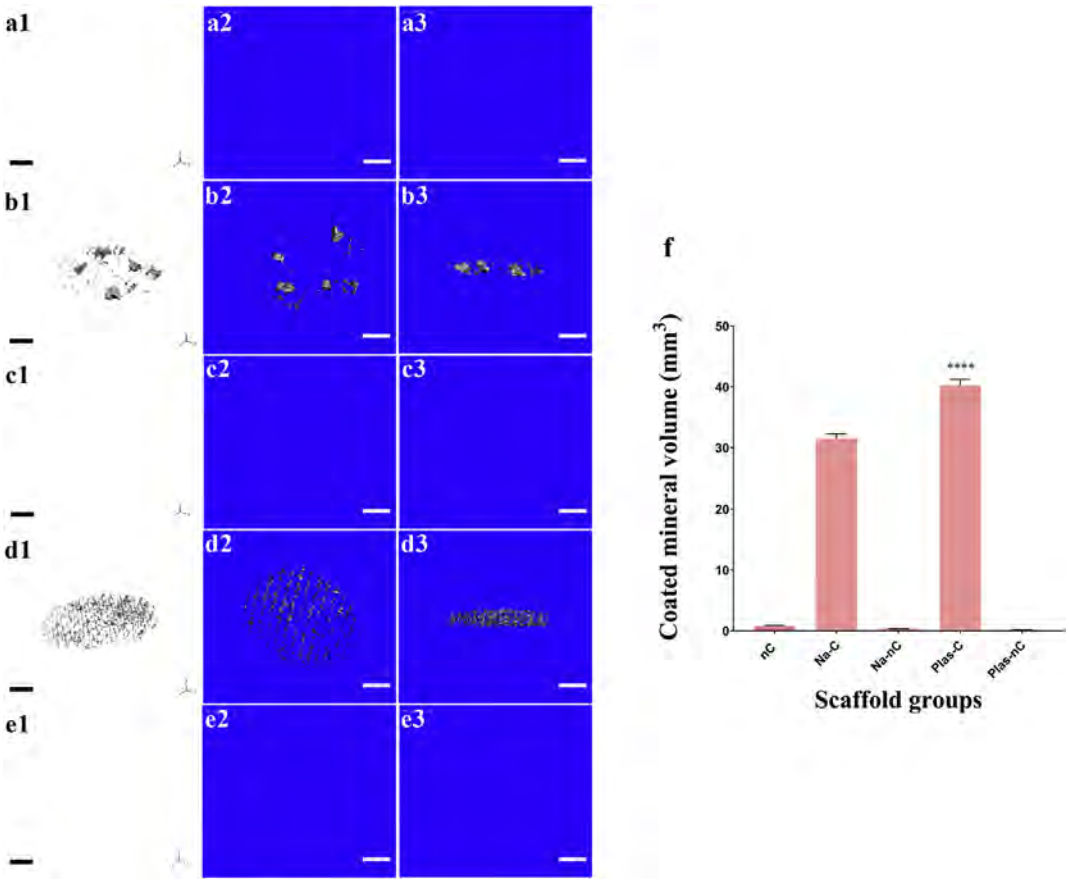

Fig. 7. μ-CT analysis of coated and non-coated PCL scaffolds (1,2) Top view; (3) Saggital section (Scale bar = 1 mm). (a) nC; (b) Na−C; (c) Na-nC; (d) Plas-C; (e) Plas-nC. (f) Total coated mineral volume. ****$p \leq 0.0001$.

influenced the solubility depending on the crystallinity and its size. The changing structures can be associated with the different pH and temperature conditions. Previous studies showed the stability of the crystal particles of coated scaffold can be modified according to the pH and temperature of the implanted site [2]. The brushite structure of the Plas-C scaffolds tends to form to HAP or TTCP, by changing the acidity or basicity of the environment. For example, in a neutral state, TCP can convert to HAP. But under acidic pH, TCP will change to a brushite structure [39]. However, the *most stable* phase of CaP at neutral pH in the human body is HAP which is the *main constituent* of bone tissue [40].

Among the different crystal structures, crystals with larger sizes have lower solubility because of the reduction in surface area [41]. Although both Plas-C and Na−C scaffolds contained halite and brushite crystal structures, the smallest crystal size was found for Plas-C scaffolds. Previous studies have shown low crystallinity and a finer crystal size can increase solubility [42] suggesting Plas-C scaffolds might have higher solubility in contrast to Na−C scaffolds. The stability and solubility of the CaP minerals reduce in order from brushite to TTCP and HAP [43]. However, Jang et al. reported higher stability of brushite in an acidic media compared to a neutral environment or alkaline as it transforms into apatitic calcium phosphate (Ap-CaP) [44]. Previous studies demonstrated the advantages of brushite within β-tricalcium phosphate (β-TCP) and monocalcium phosphate monohydrate (MCPM) for dental paste formulations and injectable orthopedics because of the high solubility of brushite. Also, the combination of brushite matrix and β-TCP granule microstructures confirmed rapid bone formation in contrast to HAP cements on the market [45]. In addition, the cubic halite crystals were detected in both Plas-C and Na−C scaffolds but in larger sizes for Na−C scaffolds. However, the higher percentage of brushite crystals enriched in Ca and P elements was confirmed in Plas-C scaffolds by EDS and XRD.

Published studies showed that larger halite crystals which results from lower temperature, reduction of free energy of the solution or the high concentration of solute can lower solubility due to less surface area contact with the solvent [46]. Release of calcium and phosphate minerals decrease with greater crystal size and higher crystallinity [47]. Therefore, there would be higher solubility of the CaP coating for Plas-C scaffolds in comparison to Na−C due to smaller crystal size.

Since the average crystal size has an impressive effect on the mechanical properties of the coated scaffolds, the tensile strength of Plas-C scaffolds showed higher Youngs modulus, elongation break% and tensile strength values between all the treated samples. Previous reports demonstrated a weak compressive strength of brushite in comparison to HAP because of more resorbable properties [47]. Both Plas-C and Na−C scaffolds showed an increase in tensile modulus compared to Plas-nC and Na-nC scaffolds similar to the study of Al-Munajjed et al. where higher mechanical properties with collagen/calcium-phosphate composite scaffolds were noted when compared to the collagen only scaffold [48]. Although Plas-C samples formed brushite crystal structures, their smaller average crystal size created a dense layer of CaP which lead to better overall mechanical properties. This is in agreement with the study of Obayi et al. who reported the mechanical tensile strength of samples increased with decreasing crystal size due to the Hall-Petch relationship [49].

Please cite this article as: N. Abbasi et al., Calcium phosphate stability on melt electrowritten PCL scaffolds, Journal of Science: Advanced Materials and Devices, https://doi.org/10.1016/j.jsamd.2020.01.001

5. Conclusion

Following O_2–Ar plasma and NaOH surface modification, an apatite mineral layer was precipitated onto the surface of MEW PCL scaffolds by immersing them in simulated body fluid. The study showed that plasma pre-treatment affords a uniform and homogeneous CaP coating with a thin layer of mineral deposition. Although XRD analysis showed that both Plas-C and Na–C scaffolds include brushite and halite structures, the halite structure was found primarily in Na–C scaffolds whereas a mixture of brushite and biphasic combinations of HAP and TTCP were found in Plas-C scaffolds. Furthermore the crystal size was also smaller in Plas-C scaffolds. Mechanical characterization indicated Plas-C scaffolds were stronger compared to the other treated scaffolds, but did lose some integrity compared to the untreated control scaffold. Plas-C scaffolds may have more stability of the CaP minerals due to the higher percentage of brushite and HAP suggesting that the plasma treatment is the most suitable for further development of MEW fibres for bone regeneration applications.

Declaration of Competing Interest

The authors declare that they have no known competing financial interests or personal relationships that could have appeared to influence the work reported in this paper.

Acknowledgments

Naghmeh Abbasi was sponsored by a scholarship from Griffith University, Australia. This study is part of her PhD research project being carried out at Griffith University. The authors would like to express their gratitude to Institute of Health and Biomedical Innovation (IHBI) and the Central Analytical Research Facility (CARF) of QUT, Australia, for providing some facilities and technical support for this study, along with Dr. Abdalla Abdal-hay for his advice and general supervision of this research. We want to acknowledge and thank Alan White and Niloofar Ordou for their technical support.

Appendix A. Supplementary data

Supplementary data to this article can be found online at https://doi.org/10.1016/j.jsamd.2020.01.001.

References

[1] M.C. Moran, G. Ruano, F. Cirisano, M. Ferrari, Mammalian cell viability on hydrophobic and superhydrophobic fabrics, Mater. Sci. Eng. C-Mater. 99 (2019) 241–247, https://doi.org/10.1016/j.msec.2019.01.088.
[2] P. Chocholata, V. Kulda, V. Babuska, Fabrication of scaffolds for bone-tissue regeneration, Materials 12 (4) (2019), https://doi.org/10.3390/ma12040568.
[3] N. Recek, Biocompatibility of plasma-treated polymeric implants, Materials 12 (2) (2019), https://doi.org/10.3390/ma12020240.
[4] F. Hajiali, S. Tajbakhsh, A. Shojaei, Fabrication and properties of polycaprolactone composites containing calcium phosphate-based ceramics and bioactive glasses in bone tissue engineering: a review, Polym. Rev. 58 (1) (2018) 164–207, https://doi.org/10.1080/15583724.2017.1332640.
[5] G. Marenzi, G. Spagnuolo, J.C. Sammartino, R. Gasparro, A. Rebaudi, M. Salerno, Micro-scale surface patterning of titanium dental implants by anodization in the presence of modifying salts, Materials 12 (11) (2019), https://doi.org/10.3390/ma12111753.
[6] L. Huang, B. Zhou, H.Y. Wu, L. Zheng, J.M. Zhao, Effect of apatite formation of biphasic calcium phosphate ceramic (BCP) on osteoblastogenesis using simulated body fluid (SBF) with or without bovine serum albumin (BSA), Mater. Sci. Eng. C-Mater. 70 (2017) 955–961, https://doi.org/10.1016/j.msec.2016.05.115.
[7] A. Nandakumar, L. Yang, P. Habibovic, C. van Blitterswijk, Calcium phosphate coated electrospun fiber matrices as scaffolds for bone tissue engineering, Langmuir 26 (10) (2010) 7380–7387, https://doi.org/10.1021/la904406b.
[8] G.B. Wasilewski, M.G. Vervloet, L.J. Schurgers, The bone-vasculature Axis: calcium supplementation and the role of Vitamin K, Front. Cardiovasc. Med. 6 (2019) 6, https://doi.org/10.3389/fcvm.2019.00006.
[9] D. Meng, L. Dong, Y. Yuan, Q. Jiang, In vitro and in vivo analysis of the biocompatibility of two novel and injectable calcium phosphate cements, Regen. Biomater. 6 (1) (2019) 13–19, https://doi.org/10.1093/rb/rby027.
[10] P. Oberbek, T. Bolek, A. Chlanda, S. Hirano, S. Kusnieruk, J. Rogowska-Tylman, G. Nechyporenko, V. Zinchenko, W. Swieszkowski, T. Puzyn, Characterization and influence of hydroxyapatite nanopowders on living cells, Beilstein J. Nanotechnol. 9 (2018) 3079–3094, https://doi.org/10.3762/bjnano.9.286.
[11] A.J. Ambard, L. Mueninghoff, Calcium phosphate cement: review of mechanical and biological properties, J. Prosthodont. 15 (5) (2006) 321–328, https://doi.org/10.1111/j.1532-849X.2006.00129.x.
[12] S. Beaufils, T. Rouillon, P. Millet, J. Le Bideau, P. Weiss, J.P. Chopart, A.L. Daltin, Synthesis of calcium-deficient hydroxyapatite nanowires and nanotubes performed by template-assisted electrodeposition, materials science & engineering, Mater. Sci. Eng. C 98 (2019) 333–346, https://doi.org/10.1016/j.msec.2018.12.071.
[13] X. Li, T. Song, X. Chen, M. Wang, X. Yang, Y. Xiao, X. Zhang, Osteoinductivity of porous biphasic calcium phosphate ceramic spheres with nanocrystalline and their efficacy in guiding bone regeneration, ACS Appl. Mater. Interfaces 11 (4) (2019) 3722–3736, https://doi.org/10.1021/acsami.8b18525.
[14] V. Huynh, N.K. Ngo, T.D. Golden, Surface activation and pretreatments for biocompatible metals and alloys used in biomedical applications, Int. J. Biomater. Res. Eng. (2019) 3806504, https://doi.org/10.1155/2019/3806504.
[15] H. Moghadas, M.S. Saidi, N. Kashaninejad, N.T. Nguyen, A high-performance polydimethylsiloxane electrospun membrane for cell culture in lab-on-a-chip, Biomicrofluidics 12 (2) (2018), https://doi.org/10.1063/1.5021002.
[16] R. Ghobeira, C. Philips, H. Declercq, P. Cools, N. De Geyter, R. Cornelissen, R. Morent, Effects of different sterilization methods on the physico-chemical and bioresponsive properties of plasma-treated polycaprolactone films, Biomed. Mater. 12 (1) (2017), https://doi.org/10.1088/1748-605X/aa51d5.
[17] W.C. Lin, N.A.M. Razali, Temporary wettability tuning of PCL/PDMS micro pattern using the plasma treatments, Materials 12 (4) (2019), https://doi.org/10.3390/ma12040644.
[18] R.R. Phiri, O.P. Oladijo, H. Nakajima, A. Rattanachata, E.T. Akinlabi, Structural and morphological dataset for rf-sputtered WC-Co thin films using synchrotron radiation methods, Data Brief 25 (2019), https://doi.org/10.1016/j.dib.2019.104383.
[19] J. Jaroszewicz, J. Idaszek, E. Choinska, K. Szlazak, A. Hyc, A. Osiecka-Iwan, W. Swieszkowski, S. Moskalewski, Formation of calcium phosphate coatings within polycaprolactone scaffolds by simple, alkaline phosphatase based method, Mater. Sci. Eng. C-Mater. 96 (2019) 319–328, https://doi.org/10.1016/j.msec.2018.11.027.
[20] W. Chen, Y.P. Liu, L.X. Yang, J.T. Wu, Q.S. Chen, Y. Zhao, Y. Wang, X.L. Du, Difference in anisotropic etching characteristics of alkaline and copper based acid solutions for single-crystalline Si, Sci. Rep.-UK 8 (2018), https://doi.org/10.1038/s41598-018-21877-x.
[21] X.R. Li, J.W. Xie, X.Y. Yuan, Y.N. Xia, Coating electrospun poly(epsilon-caprolactone) fibers with gelatin and calcium phosphate and their use as biomimetic scaffolds for bone tissue engineering, Langmuir 24 (24) (2008) 14145–14150, https://doi.org/10.1021/la802984a.
[22] A.S. Zviagin, R.V. Chernozem, M.A. Surmeneva, M. Pyeon, M. Frank, T. Ludwig, P. Tutacz, Y.F. Ivanov, S. Mathur, R.A. Surmenev, Enhanced piezoelectric response of hybrid biodegradable 3D poly(3-hydroxybutyrate) scaffolds coated with hydrothermally deposited ZnO for biomedical applications, Eur. Polym. J. 117 (2019) 272–279, https://doi.org/10.1016/j.eurpolymj.2019.05.016.
[23] P.A. Mouthuy, A. Crossley, H. Ye, Fabrication of calcium phosphate fibres through electrospinning and sintering of hydroxyapatite nanoparticles, Mater. Lett. 106 (2013) 145–150, https://doi.org/10.1016/j.matlet.2013.04.110.
[24] S.E. Noriega, G.I. Hasanova, M.J. Schneider, G.F. Larsen, A. Subramanian, Effect of fiber diameter on the spreading, proliferation and differentiation of chondrocytes on electrospun chitosan matrices, Cells Tissues Organs 195 (3) (2012) 207–221, https://doi.org/10.1159/000325144.
[25] G. Iviglia, S. Kargozar, F. Baino, Biomaterials, current strategies, and novel nano-technological approaches for periodontal regeneration, J. Funct. Biomater. 10 (1) (2019), https://doi.org/10.3390/jfb10010003.
[26] C.E. Wilson, J.D. de Bruijn, C.A. van Blitterswijk, A.J. Verbout, W.J. Dhert, Design and fabrication of standardized hydroxyapatite scaffolds with a defined macro-architecture by rapid prototyping for bone-tissue-engineering research, J. Biomed. Mater. Res. 68 (1) (2004) 123–132, https://doi.org/10.1002/jbm.a.20015.
[27] T. Kokubo, S. Yamaguchi, Simulated body fluid and the novel bioactive materials derived from it, J. Biomed. Mater. Res. 107 (5) (2019) 968–977, https://doi.org/10.1002/jbm.a.36620.
[28] C. Pierre, G. Bertrand, C. Rey, O. Benhamou, C. Combes, Calcium phosphate coatings elaborated by the soaking process on titanium dental implants: surface preparation, processing and physical-chemical characterization, Dent. Mater. 35 (2) (2019) E25–E35, https://doi.org/10.1016/j.dental.2018.10.005.
[29] P. Nguyen-Trig, F. Altiparmak, N. Nguyen, L. Tuduri, C.M. Ouellet-Plamondon, R.E. Prud'homme, Robust superhydrophobic cotton fibers prepared by simple dip-coating approach using chemical and plasma-etching pretreatments, ACS Omega 4 (4) (2019) 7829–7837, https://doi.org/10.1021/acsomega.9b00688.

Please cite this article as: N. Abbasi et al., Calcium phosphate stability on melt electrowritten PCL scaffolds, Journal of Science: Advanced Materials and Devices, https://doi.org/10.1016/j.jsamd.2020.01.001

[30] M. Yamamoto, T. Matsumae, Y. Kurashima, H. Takagi, T. Suga, T. Itoh, E. Higurashi, Comparison of argon and oxygen plasma treatments for ambient room-temperature wafer-scale Au-Au bonding using ultrathin Au films, Micromachines-Basel 10 (2) (2019), https://doi.org/10.3390/mi10020119.

[31] T. Desmet, R. Morent, N. De Geyter, C. Leys, E. Schacht, P. Dubruel, Nonthermal plasma technology as a versatile strategy for polymeric biomaterials surface modification: a review, Biomacromolecules 10 (9) (2009) 2351–2378, https://doi.org/10.1021/bm900186s.

[32] I.A. Khlusov, Y. Dekhtyar, Y.P. Sharkeev, V.F. Pichugin, M.Y. Khlusova, N. Polyaka, F. Tjulkins, V. Vendinya, E.V. Legostaeva, L.S. Litvinova, V.V. Shupletsova, O.G. Khaziakhmatova, K.A. Yurova, K.A. Prosolov, Nanoscale electrical potential and roughness of a calcium phosphate surface promotes the osteogenic phenotype of stromal cells, Materials 11 (6) (2018), https://doi.org/10.3390/ma11060978.

[33] V. Anand, R. Thomas, K.H. Thulasi Raman, M.R. Gowravaram, Plasma-Induced Polymeric Coatings. Non-Thermal Plasma Technology for Polymeric Materials, Elsevier, 2018, pp. 129–157.

[34] A.K. Kumar, S. Sharma, Recent updates on different methods of pretreatment of lignocellulosic feedstocks: a review, Bioresour. Bioprocess. 4 (1) (2017) 7, https://doi.org/10.1186/s40643-017-0137-9.

[35] N. Luickx, N. Van den Vreken, W. D'Oosterlinck, L. Van der Schueren, H. Declercq, K. De Clerck, M. Cornelissen, R. Verbeeck, Optimization of the activation and nucleation steps in the precipitation of a calcium phosphate primer layer on electrospun poly(varepsilon-caprolactone), J. Biomed. Mater. Res. 103 (2) (2015) 511–524, https://doi.org/10.1002/jbm.a.35191.

[36] W. Wang, G. Caetano, W.S. Ambler, J.J. Blaker, M.A. Frade, P. Mandal, C. Diver, P. Bartolo, Enhancing the hydrophilicity and cell attachment of 3D printed PCL/graphene scaffolds for bone tissue engineering, Materials (Basel) 9 (12) (2016), https://doi.org/10.3390/ma9120992.

[37] A. Kobayashi, T. Kuroda, H. Kimura, A. Inoue, Effect of Zr on microstructure of metallic glass coatings prepared by gas tunnel type plasma spraying, J. Nanosci. Nanotechnol. 12 (6) (2012) 4883–4886, https://doi.org/10.1166/jnn.2012.4944.

[38] Y. Li, C. Liao, S.C. Tjong, Synthetic biodegradable aliphatic polyester nanocomposites reinforced with nanohydroxyapatite and/or graphene oxide for bone tissue engineering applications, Nanomaterials (Basel) 9 (4) (2019), https://doi.org/10.3390/nano9040590.

[39] L. Morejon, J.A. Delgado, A. Antunes Ribeiro, M. Varella de Oliveira, E. Mendizabal, I. Garcia, A. Alfonso, P. Poh, M. van Griensven, E.R. Balmayor, Development, characterization and in vitro biological properties of scaffolds fabricated from calcium phosphate nanoparticles, Int. J. Mol. Sci. 20 (7) (2019), https://doi.org/10.3390/ijms20071790.

[40] N.A.S. Mohd Pu'ad, P. Koshy, H.Z. Abdullah, M.I. Idris, T.C. Lee, Syntheses of hydroxyapatite from natural sources, Heliyon 5 (5) (2019), e01588, https://doi.org/10.1016/j.heliyon.2019.e01588.

[41] K. Zheng, Z. Lin, M. Capece, K. Kunnath, L. Chen, R.N. Dave, Effect of particle size and polymer loading on dissolution behavior of amorphous griseofulvin powder, J. Pharmaceut. Sci. 108 (1) (2019) 234–242, https://doi.org/10.1016/j.xphs.2018.11.025.

[42] X. Pan, T. Julian, L. Augsburger, Increasing the dissolution rate of a low-solubility drug through a crystalline-amorphous transition: a case study with indomethacin [correction of indomethicin], Drug Dev. Ind. Pharm. 34 (2) (2008) 221–231, https://doi.org/10.1080/03639040701580606.

[43] S. Shaddel, S. Ucar, J.P. Andreassen, S.W. Osterhus, Enhancing efficiency and economics of phosphorus recovery process by customizing the product based on sidestream characteristics - an alternative phosphorus recovery strategy, Water Sci. Technol.: J. Int. Assoc. Water Pollut. Res. 79 (9) (2019) 1777–1789, https://doi.org/10.2166/wst.2019.178.

[44] H.L. Jang, G.B. Zheng, J. Park, H.D. Kim, H.R. Baek, H.K. Lee, K. Lee, H.N. Han, C.K. Lee, N.S. Hwang, J.H. Lee, K.T. Nam, In vitro and in vivo evaluation of whitlockite biocompatibility: comparative study with hydroxyapatite and beta-tricalcium phosphate, Adv. Health Mater. 5 (1) (2016) 128–136, https://doi.org/10.1002/adhm.201400824.

[45] D. Apelt, F. Theiss, A.O. El-Warrak, K. Zlinszky, R. Bettschart-Wolfisberger, M. Bohner, S. Matter, J.A. Auer, B. von Rechenberg, In vivo behavior of three different injectable hydraulic calcium phosphate cements, Biomaterials 25 (7–8) (2004) 1439–1451, https://doi.org/10.1016/j.biomaterials.2003.08.073.

[46] L. Sun, C.C. Berndt, K.A. Khor, H.N. Cheang, K.A. Gross, Surface characteristics and dissolution behavior of plasma-sprayed hydroxyapatite coating, J. Biomed. Mater. Res. 62 (2) (2002) 228–236, https://doi.org/10.1002/jbm.10315.

[47] E.A. Abou Neel, A. Aljabo, A. Strange, S. Ibrahim, M. Coathup, A.M. Young, L. Bozec, V. Mudera, Demineralization-remineralization dynamics in teeth and bone, Int. J. Nanomed. 11 (2016) 4743–4763, https://doi.org/10.2147/Ijn.S107624.

[48] A.A. Al-Munajjed, F.J. O'Brien, Influence of a novel calcium-phosphate coating on the mechanical properties of highly porous collagen scaffolds for bone repair, J. Mech. Behav. Biomed. Mater. 2 (2) (2009) 138–146, https://doi.org/10.1016/j.jmbbm.2008.05.001.

[49] C.S. Obayi, R. Tolouei, A. Mostavan, C. Paternoster, S. Turgeon, B.A. Okorie, D.O. Obikwelu, D. Mantovani, Effect of grain sizes on mechanical properties and biodegradation behavior of pure iron for cardiovascular stent application, Biomatter 6 (2016), e959874, https://doi.org/10.4161/21592527.2014.959874.

Please cite this article as: N. Abbasi et al., Calcium phosphate stability on melt electrowritten PCL scaffolds, Journal of Science: Advanced Materials and Devices, https://doi.org/10.1016/j.jsamd.2020.01.001